On the Origin of Size-Dependent and Size-Independent Crystal Growth: Influence of Advection and Diffusion

Daniel E. Kile* and D. D. Eberl
U.S. Geological Survey
3215 Marine St. – Ste. E-127
Boulder, Colorado 80303-1066
*email: dekile@usgs.gov

Abstract

Crystal growth experiments were conducted using potassium alum and calcite crystals in aqueous solution under both non-stirred and stirred conditions to elucidate the mechanism for size-dependent (proportionate) and size-independent (constant) crystal growth. Growth by these two laws can be distinguished from each other because the *relative* size difference between crystals is maintained during proportionate growth, leading to a constant crystal size variance (β^2) for a crystal size distribution (CSD) as the mean size increases. The *absolute* size difference between crystals is maintained during constant growth, resulting in a decrease in size variance. Results of these experiments show that for centimeter-size alum crystals, proportionate growth occurs in stirred systems, whereas constant growth occurs in non-stirred systems. Accordingly, the mechanism for proportionate growth is hypothesized to be related to the supply of reactants to the crystal surface by advection, whereas constant growth is related to supply by diffusion. Paradoxically, micron-size calcite crystals showed proportionate growth both in stirred and in non-stirred systems. Such growth presumably results from the effects of convection and Brownian motion which promote an advective environment and hence proportionate growth for minute crystals in non-stirred systems, thereby indicating the importance of solution velocity relative to crystal size. Calcite crystals grown in gels, where fluid motion was minimized, showed evidence for constant, diffusion-controlled growth. Additional investigations of CSDs of naturally occurring crystals indicate that proportionate growth is by far the most common growth law, thereby suggesting that advection, rather than diffusion, is the dominate process for supplying reactants to crystal surfaces.

Introduction

An understanding of the mechanisms of crystal growth and resultant crystal size distributions (CSDs) is important because geological information can be deduced from the shapes of CSDs if the relations between these shapes and the underlying geological processes are understood. Although a considerable amount of research has focused on studying crystal growth based on CSDs, results have been inconsistent, leading to contradictory interpretations of crystal growth mechanisms. Attempts to model crystal growth mathematically have fared little better; they often fail to predict either the commonly observed lognormal size distribution or the associated crystal size variance (Eberl et al. 2002a).

One controversy surrounding earlier studies involves interpretation of crystal growth in terms of size-independent (constant) vs. size-dependent (proportionate) growth (Eberl et al. 2002a). This paper will explore the origins of these two growth mechanisms, how these types of growth affect the CSD shape, and how they can be affected by environmental conditions. These growth mechanisms, investigated with experiments using potassium alum and calcite crystals grown in both unstirred and stirred aqueous solutions, are presumed to have occurred under conditions of supply-controlled growth, when the rate-controlling step is the supply of reactants to the crystal surface, either by diffusion or by advection. This type of growth contrasts with surface-controlled growth, where the supply of reactants exceeds the growth rate.

Three CSD shapes commonly are formed early in the crystallization process: lognormal, asymptotic, and a "universal steady-state" shape consistent with a process of Ostwald ripening (Eberl et al. 1998; Kile et al. 2000). The initial CSD shape then may be modified during subsequent supply-controlled growth that can be described by constant growth, by proportionate growth, or by some combination of the two; usually it is during this phase of growth when most of the crystal mass is added. Several other growth laws are possible (see below), but have not been detected in our experiments.

Growth Equations

Constant growth was described by McCabe in 1929, who postulated a "ΔL law", whereby crystallographically equivalent faces on similar crystals would grow at the same rate. This growth law has been approximated by dr/dt = k (Nordeng and Sibley 1996; Kile et al. 2000), where r is the crystal radius and k is a constant.

Constant (size-independent) growth can be simulated mathematically by

$$X_{j+1} = X_j + k_j, \qquad (1)$$

where X_j is the crystal diameter after j time intervals, or steps (or j iterations of the equation), and k_j is a constant that is approximately equal for crystals of all sizes after growth for a given interval of time, but not necessarily constant through time. In other words, Equation 1 states that all of the geometrically similar crystals in a system, regardless of their size, will grow by the same linear amount (i.e., add a layer of material with the same thickness) during a given time interval. The origin of this type of growth has been ascribed to several crystal growth mechanisms, including surface-reaction-limited polynuclear growth and spiral growth (Nielson 1964; Ohara and Reid 1973; Nordeng and Sibley, 1996). These mechanisms are consistent with classical spiral crystal growth theory as described by Burton, Cabrera and Frank (i.e., the BCF model as described in Bennema 1967, 1984), and with the three-step model of crystal growth (e.g., as cited in Mullin 1972), whereby growth proceeds by a two-step process: (1) a diffusion step, wherein growth is regulated by a boundary layer, the thickness of which is controlled by solution velocity, etc., and (2) a surface integration step, with rates being controlled by the density of spiral growth centers or hillocks that provide energetically favorable sites for monolayer deposition. Surface integration rates also can be controlled by crystal solubility and by environmental factors such as solution temperature. The overall growth rate for a given crystal is dependent on which of these two steps becomes rate limiting.

The constant growth law has been the foundation of many attempts to model crystal growth; it underlies the population balance equation used in petrology (e.g., Marsh 1988), the growth models proposed by Kretz (1966), the classic Johnson, Mehl, and Avrami (JMA) approach (discussed in Kirkpatrick 1981), and the population balance model proposed by McCoy (2001), among others. However, there is a growing body of literature that contradicts the constant growth law. Proportionate growth, evidenced in both natural and synthetic crystal systems, appears to better account for observed CSDs, and has been found in a variety of synthetic crystal systems studied by Canning and Randolph (1967), Mullin and Gaska (1969), Garside and Jancic (1976), Jones et al. (1986), Tai and Yu (1989), and Tai et al. (1993).

Proportionate growth also has been noted in geologic systems, e.g., Nordeng and Sibley (1996), Kile and Eberl (1999), Makowitz and Sibley (1999, 2001), and Meth and Carlson (2002). Simple mathematical arguments that favor proportionate rather than constant growth for most natural systems have been presented by Eberl et al. (2002a).

Proportionate (size-dependent) growth can be approximated by

$$X_{j+1} = X_j + k_j X_j. \qquad (2)$$

This equation indicates that the amount a crystal will grow through a certain time interval will be proportional to its initial size. Proportionate growth (which has been approximated as dr/dt = kr) has been ascribed to an accelerated solution velocity around larger crystals (McCabe and Stevens 1951), to a greater density of dislocation defects on the surfaces of larger crystals (Garside et al. 1976; Ristic et al. 1991; Jones and Larson 1999, 2000), and to the effects of lattice strain as a function of crystal size (Ristic et al. 1997; Jones and Larson 1999, 2000).

Equation 2, and by analogy Equation 1, are considered to be approximations because k_j may contain inherent randomness. This randomness can be expressed using an equation similar to Equation 2, known as the Law of Proportionate Effect (LPE), where k_j is replaced by a random number (ε_j) that varies between limits (usually 0 to 1). Such randomness is required to produce a lognormal CSD, which is one of the most commonly observed CSD shapes. A computer program (Galoper; Eberl et al. 2000) uses the LPE to simulate the development of CSDs for many types of minerals (Eberl et al. 1998; Kile and Eberl 1999; Kile et al. 2000; Srodon et al. 2000) by both surface- and supply-controlled growth. For example, supply-controlled growth can be simulated by mathematically limiting the volume available for growth during each iteration of the LPE. The mathematical effect of limiting supply is that ε_j will vary between zero and a very small number; growth approximates dr/dt = kr after many growth cycles.

Constant growth (Eq. 1) can be distinguished from proportionate growth (Eq. 2) by the effects these growth mechanisms have on the shapes of CSDs. Constant growth maintains the *absolute* size difference between crystals as mean size increases, because such growth is described by *adding* the same layer thickness to each crystal per unit time. For example, if one crystal is two microns smaller than another at the beginning of growth, this two-micron size difference will be maintained throughout the growth process. Proportionate growth, however, maintains the *relative* size difference between crystals because growth is modeled by *multiplying* each size by a constant. In other words, if one crystal is twice the size of another at the beginning of proportionate growth, it will remain twice the size as growth proceeds.

The overall effect of Equation 1 on the CSD is to cause its natural log-based crystal size variance (β^2) for a given population of crystals to decrease as mean size increases, whereas growth by Equation 2 leads to a constant β^2 for supply-controlled growth. Only proportionate growth can generate and maintain a lognormal CSD, and only proportionate growth can maintain the theoretical shape for the universal steady-state curve expected from Ostwald ripening, after ripening (which occurs only at small crystal sizes) has ceased (Kile et al. 2000; Eberl et al. 2002a). Galoper simulation shows, however, that constant growth will cause the lognormal and Ostwald CSDs to narrow with respect to their corresponding theoretical curves as growth proceeds (Eberl et al. 2002a).

Experimental

We hypothesized that proportionate growth is likely due to a hydrodynamic effect that results from a faster solution velocity around larger crystals (analogous to the Bernoulli effect), as documented, for example, by McCabe and Stevens (1951) and Mullin and Gaska (1969). In free-flowing systems, larger crystals also could cause a greater disturbance to flow, leading to greater turbulence and therefore to greater mixing in the vicinity of the crystal. To test the hypothesis, the rate of crystal growth was studied in both non-stirred and in stirred systems for two minerals: (1) centimeter-size potassium alum crystals having different initial sizes, for which the growth rate of each crystal could be measured based on weight change, and (2) micron-size calcite crystals, for which growth rate could be determined by direct microscopic measurement of size to determine the CSD shape. Three types of experiments were designed accordingly to assess the effect of growth conditions on growth law:

1. Alum crystals were grown by evaporation, under both static (unstirred) and dynamic (stirred) conditions, in multi-crystal systems.
2. Calcite crystals were grown in bulk aqueous solution without stirring; results from this experiment were compared to results from stirred experiments conducted by Kile et al. (2000).
3. Calcite crystals were grown in a silica-gel medium to minimize the effects of solution advection on crystal growth.

Also investigated were two natural occurrences of minerals thought to have grown in static systems. Therefore, the shapes of their CSDs should reflect to some extent crystal growth that is constrained by diffusion-limited reactant supply. The first occurrence is calcite crystals found as small rhombohedra (mean diameter 13.5 μm) within minute fractures in a "molar tooth" structure in the Precambrian, Proterozoic Helena Formation of the Middle Belt Carbonate,

Montana (Furniss et al. 1998). The second occurrence is crystals (possibly greigite, an iron sulfide) that grew within pennate diatom silica exoskeletons from a single species found in sediment core samples (at a depth of 4 to 5 cm) collected from Pyramid Lake, Nevada. These crystals (mean diameter = 3.6 μm) presumably formed in reducing environments within the diatoms in response to decomposing organic matter in a recently deceased organism.

The growth of individual crystals is emphasized in the present study because of complications inherent in batch methods of crystallization, e.g., mixed-suspension mixed-product removal (MSMPR) or fluidized-bed crystallizers. In contrast to single-crystal studies, agitated batch crystallizers obscure the growth mechanism and rates for individual crystals. For example, agitation in batch crystallizers has been shown to be a source of secondary nucleation. Moreover, crystal damage resulting from particle collisions can presumably lead to additional growth spirals and consequent apparent size-dependent growth effects; this effect may be magnified for larger crystals which are more likely to have increasingly energetic collisions.

Alum was chosen for the present work because its high solubility gives a substantial yield per unit volume of water evaporated, and because of the relative ease of growing large crystals with minimal imperfections. An additional advantage is that crystal mass can easily be quadrupled during the course of the experiment, minimizing measurement errors. The disadvantage in working with a few large crystals is that randomness inherent in the system (e.g., as caused by variations in flow rates around crystals, heterogeneities in solution composition and in crystal surface structure, etc.) may tend to obscure growth tendencies when only a few crystals are measured.

Alum crystals [$KAl(SO_4)_2 \cdot 12H_2O$; A.C.S. Certified Reagent, Fisher Scientific] were grown by evaporation from saturated aqueous solution, using procedures modified from Holden and Singer (1960). Both temperature-controlled and ambient-temperature experiments were carried out. Temperature-controlled experiments were conducted using a water-jacketed crystallization vessel of about 6L capacity which accommodated from 10 to 12 crystals (Fig. 1). Temperature control was maintained with a circulating refrigerated/heated water bath, with a temperature setpoint of 29.7 ± 0.2 °C. Ambient temperature experiments were carried out in a 4-L single-wall glass chromatography vessel, which held from 4 to 6 crystals. Crystals were suspended from a Plexiglas platform by nylon threads, and also mounted with Epoxy on 2-mm diameter glass rods (using a pre-drilled hole in the crystal) which were attached to a Plexiglas plate on the bottom of the vessel. The solutions in these experiments were stirred with a variable speed stirrer and

propeller that was positioned in the center of the vessel; the speed was varied between 122 and 272 RPM. One experiment was stirred using a magnetic bar (see Table 1).

Saturated alum solutions were filtered (Gelman Metricel® 45 μm membrane filter) and equilibrated for approximately 24 h prior to the addition of seed crystals. Supersaturation was maintained at a constant level through controlled evaporation, the rate of which was adjusted by raising or lowering the height of a Plexiglas lid on the water-jacketed crystallizing vessel, or by varying the distance between two shutters that were positioned on top of a hole in this lid. For the unstirred experiments, conducted at about 29 °C, the rate of evaporation varied from 1.81 to 6.06 mL/h. The rate of evaporation for stirred experiments, conducted at 29.7 °C, varied from 6.14 to 7.17 mL/h.

The level of supersaturation (σ), monitored for most experiments, is defined as:

$$\sigma = \frac{C - C^*}{C^*}, \qquad (3)$$

where C is the solution concentration and C^* is the equilibrium concentration at saturation, in g/g solution. Solution concentration was determined both gravimetrically and by refractometry. The equilibrium solution concentration was approximately 143.5 g/g solution at 29.7 °C, whereas the average solution concentration for stirred experiments was measured at 151.0 g/g solution; the average σ was therefore 0.052.

Alum, an isometric mineral, grows in a predominantly octahedral {111} form, with {100} modifications. Assuming symmetrical growth of these forms, crystal volume can be approximated from weight by modeling a spherical shape. Crystal size for alum was accordingly determined by weight, with the diameter being calculated based on crystal density (alum = 1.757).

The effect of stirring on calcite CSDs was investigated by synthesizing calcite crystals in aqueous solution by mixing equimolar solutions of $CaCl_2 \cdot 2H_2O$ and Na_2CO_3, and allowing crystallization to proceed without stirring. These experiments are in contrast to earlier experiments that documented CSDs obtained from stirred solutions (Kile et al. 2000). Accordingly, solutions of 0.00835 M $CaCl_2.2H_2O$ and Na_2CO_3, with 0.50 M NaCl to inhibit vaterite formation, and 0.05 M KNO_3 to control ionic strength, were mixed and filled to overflowing in a 120 mL vessel, which was capped and allowed to sit without stirring for approximately 17 h. The calcite precipitate then was filtered through a 0.45 mm cellulose nitrate filter (Millipore) and air dried. Crystals were mounted in Canada balsam on a glass slide, and the

crystal size was measured across the long diagonal of the rhombohedral form. The diameters of the micron-size calcite crystals were measured using a polarized-light microscope with a calibrated filar micrometer ocular. Microscopic measurements eliminate errors that can be introduced when using automated methods. For example, laser-light scattering instruments such as a Coulter counter may measure crystal aggregates as a single crystal (Kile et al. 2000), leading to an overestimation of size and consequently to inaccurate determinations of CSD shape.

The relative initial concentration of the solution (Ω) was approximately 500, where $\Omega = Q/K_{sp}$, and $Q = [H^+]/[Ca^{2+}][HCO_3^-]$. Values in brackets refer to activities in solution, and K_{sp} is the solubility product of calcite crystals in the standard state. Further details are given in Kile et al. (2000).

Calcite crystals also were grown in a silica-gel matrix by the method of Henisch (1988), a method that is presumed to minimize reactant transport by advection. Both a U-shaped tube and a straight column were used in these experiments. A 15-mm inside diameter U-shaped tube was partly filled with a sodium meta-silicate gel (0.2 M $Na_2SiO_3 \cdot 9H_2O$; J.T. Baker Analyzed Reagent, pH adjusted to ~7 with acetic acid). The gel, after solidifying, was overlain on one end with a 0.16 M solution of $(NH_4)_2CO_3$ (EM Science), and on the other end by a 0.16 M solution of $CaCl_2.2H_2O$ (Fisher, A.C.S.). Movement of the reactants through the gel from opposite ends of the tube ultimately resulted in crystal nucleation which was followed by growth that continued for 6 to 8 weeks. This gel method yielded macroscopic calcite crystals, the sizes of which were determined by measurement of linear dimensions from a photograph. Crystals formed within the U-shaped column occurred in two distinct Liesegang rings (Liesegang rings are characterized by a series of concentrically developed rings, with regularly developed spacings between them), each with a considerably different mean crystal size; however, there were too few crystals in one of the rings to yield an accurate CSD shape.

Sodium meta-silicate gel used in the 30-mm (inside diameter) straight column was prepared as above, with the exception that 0.16 M ammonium carbonate was incorporated into the gel. The column was partly filled with the gel, after which the gel was overlain with 0.16 M calcium chloride. Three distinct Liesegang rings were formed near the top of this column, with mean crystal sizes being progressively larger farther down the column. Crystal size was measured (using an ocular micrometer and a low-power stereomicroscope) and tabulated for populations within each ring following separation of the crystals from the gel.

CSDs were determined from crystal size data using the program CrystalCounter (Eberl et al. 2000). In general, group size was set to a minimum that mitigated the "noise" level in the plot. This criterion for the choice of group (i.e., bin) size proved to be important because the universal steady-state CSD shape that results from Ostwald ripening according to LSW theory (Lifshitz, Slyozov, and Wagner; see Eberl et al. 1998) can be deformed into a lognormal-appearing CSD if the group size is too large. The program then calculates the CSD shape, the mean crystal size, the mean of the natural logarithms of the sizes (α), and the variance of the natural logarithms of the sizes (β^2, see below). The chi-square (χ^2) test (Krumbein and Graybill 1965) and the K-S (Kolmogorov-Smirnov) test (Benjamin and Cornell 1970) were used to assess the fit of the data to theoretical and calculated CSDs. The chi-square test, which uses a differential distribution, is more stringent than the K-S test which uses a cumulative distribution; however the K-S test is useful if there are less than 10 size groups (bins) for the data, and/or if the data are noisy. These statistical tests compare CSDs of measured size distributions to theoretical lognormal distributions, and give a level of significance ranging from <1% (i.e., the CSDs are not the same) to > 10% (i.e., a high level of significance) for the K-S test, or from <1% to >20% for the chi-square test. CSDs are considered to be the same if the significance level for comparison between the measured and theoretical curves is equal to or greater than the 1% to 5% range (Exner and Lukas 1971). No conclusions regarding our data were made without statistical confirmation, which was used to indicate lognormality as well as to compare measured CSDs with simulated (Galoper) or theoretical CSDs. Probability paper commonly is used as a rapid, qualitative check on the normality of a distribution. If normal, a plot of the cumulative frequency shows a straight line; if log scales have been used, then the straight line shows that the distribution is lognormal. However, the chi-square and K-S tests are more quantitative than the graphing method because a significance level can be assigned to the fit.

Results and Discussion

Alum experiments.

Figure 2 presents results of alum crystal growth experiments for stirred (Fig. 2a) and unstirred (Fig. 2b) systems. The initial diameter for each crystal is plotted versus its amount of growth (final diameter – initial diameter). Scales for ordinate and abscissa are the same for both plots to facilitate a direct comparison. The slopes of the lines (i.e., the size-dependent effect) in Figure 2a are approximately proportional to the amount of crystal growth in a given experiment. The relevant growth parameters for these experiments are given in Table 1.

A comparison between these two plots clearly shows the effect of solution velocity as manifested by the slope of the lines. Figure 2 may indicate that proportionate growth is related to a hydrodynamic effect that depends on stirring, whereby the velocity of a liquid medium flowing around an object increases in direct proportion to the object's circumference, and, therefore, in direct proportion to its diameter. This result also is consistent with the diffusion step in the three-step model (and variations thereof) of crystal growth, whereby the boundary layer thickness may decrease as velocity increases, thereby leading to an increased growth rate for larger crystals (e.g., Canning and Randolph 1967; Abegg et al. 1968). Thus, crystal growth under stirred conditions results in proportionate growth (i.e., larger crystals tend to grow faster) according to Equation 2, whereas growth under unstirred conditions yields constant growth according to Equation 1.

Some crystals in the stirred experiments had growth rates which deviated considerably from the mean. This "noise" may be explained in part by an intrinsic randomness in the system (Eberl et al. 1998), which, as mentioned above, may result from variation in physical properties of crystals [e.g., lattice strain and dislocation density as suggested by Ristic et al. (1991, 1997), and Jones and Larson (1999, 2000)], which may lead to different inherent growth rates for individual crystals such as reported by Berglund (1983), or from a heterogeneous solution environment (e.g., variable advective currents).

Calcite experiments.

Micron-size calcite was crystallized in bulk solution without stirring to further investigate the influence of advection on proportionate growth. The CSD (Fig. 3) shows a lognormal curve (χ^2 level of significance = 5% to 10%; K-S test > 10%) with a β^2 of 0.23 (Table 2). The similarity of this plot to those generated in stirred systems (Kile et al. 2000) is evidence for proportionate growth, because this mechanism of crystal growth is the only straightforward approach which can consistently generate and maintain a lognormal CSD (Eberl et al. 2002a). Convection and Brownian motion of the crystals are the likely means for advective transport of reactants. This observation seems contrary to the finding of constant growth for the alum unstirred experiments; however, the data can be explained in terms of solution velocity relative to crystal size. Although solution motion is minimal for the calcite experiment, advective movement may be considerable in proportion to the mean crystal size (28.2 μm for calcite vs. centimeter-size for alum).

In the straight-column gel experiment, the upper and middle Liesegang rings contained the smallest- (mean = 60 μm) and medium-size (mean = 147 μm) crystals, respectively, whereas the

deepest ring contained the largest crystals (mean = 313 μm). The CSDs for the upper and middle rings follow the shape expected for Ostwald ripening according to LSW theory (Fig. 4a and 4b). Chi-square comparisons between the measured and the theoretical Ostwald CSDs yielded significance levels of 2.5%to 5% for the upper ring and <1% for the middle ring, but the K-S test yielded a significance level of >10% for both rings. The size variance (β^2) of both CSDs (0.057 and 0.064) are those expected for the theoretical shape (0.06). However, the crystals in these rings are too large to have grown entirely by Ostwald ripening which, for calcite, should be effective at low temperatures only for crystals having sizes much less than 0.1 μm (Morse and Wang 1996). Ripening is not expected for larger sizes because specific surface energy differences for such crystals are too small to drive the ripening process. Therefore, it is proposed that the initial shapes of these CSDs resulted from Ostwald ripening at very small sizes (<<100 nm, and probably <10 nm; Kile et al. 2000), and that this ripening was followed by proportionate growth which preserved the Ostwald CSD shapes as the crystals grew larger.

The CSD shape for the lowest ring (Fig. 4c) also appears to follow the Ostwald shape in that the distribution is skewed to the left; it is much narrower, however, than the Ostwald CSD, having a β^2 of 0.016 rather than the theoretical value of 0.06. If 169 μm is subtracted from each crystal size and the CSD recalculated (Fig. 4c), then the theoretical Ostwald CSD is achieved with a K-S test significance level of >10 %. This CSD shape can be attained with a proposed growth history whereby crystallization initially starts with Ostwald ripening, followed by proportionate growth, as was hypothesized for crystals in two upper rings. But when the mean size reached 144 μm for calcite in the lowest ring, the growth mechanism changed from proportionate growth to constant growth, at which time the crystals grew an additional 169 μm to their present size. The growth mechanism presumably changed because the supply of reactants changed from advective supply to diffusive supply, perhaps due to a change in porosity caused by a compression of the gel surrounding the comparatively large crystals in the lowest ring.

In the U-tube experiment, only the lowermost ring had sufficient crystals to be measured; these reacted similarly to those found in the lowest ring in the straight column. Calculations show a growth history of Ostwald ripening followed by proportionate growth which resulted in a mean crystal size of 438 μm; this was then followed by a brief period of constant growth to a mean size of 565 μm.

Natural analogs.

Most CSDs measured from natural systems show either a lognormal shape or a closely related asymptotic shape. Rarely, the Ostwald universal steady-state shape may be observed in the CSDs. As was discussed above, all of these shapes indicate proportionate growth after the formation of the initial CSD shape (e.g., Eberl et al. 1998, and references therein; Kile and Eberl 1999; Kile et al. 2000; Eberl et al. 2002a). Evidence for a constant growth mechanism appears to be rare in geologic systems. We have found only two possible isolated examples:

1. A CSD for calcite crystals that are found in minute fractures within Precambrian rocks (molar tooth structure) shows evidence for constant growth. The CSD has the negative skew expected for the Ostwald universal steady-state shape, but is much too narrow to fit an Ostwald profile because the β^2 is 0.02, rather than 0.06 that is expected for Ostwald ripening. The CSD can be simulated in the same manner as was the lowest Liesegang ring in the experiments discussed above by assuming that the Ostwald shape was modified by constant growth. The Galoper simulation (Fig. 5a) starts with nucleation and growth, followed by Ostwald ripening, then consecutively by proportionate growth and constant growth. Given this crystallization sequence, constant growth would have started when the mean crystal size was 7.5 μm, and then continued to the mean size of 13.5 μm. Subtracting 6 μm (see Eq. 1) from each crystal size exactly restores the Ostwald steady-state shape (Fig. 5b). The CSD can be simulated equally well if the last two growth stages are reversed; however, based on geological and geochemical considerations, the first growth sequence would be more likely. Because the rate of crystal growth during the constant portion of the growth history was presumably limited by ion diffusion through microfractures in a compacted marine sediment (Furniss et al. 1998), and because the Ostwald shape indicates that rapid nucleation occurred at large levels of supersaturation (Kile et al. 2000; Eberl et al. 2002b), a crystal growth history can be proposed whereby: (1) rapid nucleation followed by Ostwald ripening occurs under conditions of high supersaturation, followed by (2) a period of proportionate growth, which in turn changes to (3) constant growth as increasing sediment compaction slows the reactant supply rate.

2. CSDs for the iron sulfide crystals found within numerous diatoms (Fig. 6a) in Pyramid Lake sediments also show a narrow profile ($\beta^2 = 0.069$; Fig. 6b), perhaps indicative of constant growth; exclusion of the small bimodal peak at the left of the plot narrows the size variance of this profile even further, to 0.047. This CSD was simulated by a mechanism of nucleation and growth, followed consecutively by Ostwald ripening, proportionate growth, and constant growth. A period of constant growth is required to generate the small β^2. However, this growth sequence is speculative because there may be other reaction pathways that could generate this

CSD. The semi-permeable silica exoskeleton may have limited the influx of reactants to supply by diffusion, resulting in constant, size-independent crystal growth.

Conclusions

Experimental evidence indicates that crystal growth mechanisms are governed by the nature of the transport of reactants to the crystal surface. Accordingly, constant, size-independent growth (Eq. 1) results when reactant supply to crystal surfaces is diffusion-limited, whereas proportionate, size-dependent growth (Eq. 2) results when reactants are supplied by advection. Proportionate growth thus is expected whenever the rate of reactant supply by advection exceeds that by diffusion. Proportionate growth is evidenced by lognormal CSDs; by contrast, constant growth is evidenced by very small size variances (e.g., β^2 less than 0.06 for Ostwald-like CSDs). Thus, CSDs measured for naturally occurring minerals indicate that crystallization by constant, diffusion-controlled growth is rare.

Advection appears to control growth even in seemingly stagnant conditions, e.g., within miarolitic cavities and septarian concretions, where lognormal CSDs have been recorded (Kile and Eberl, 1999). Therefore, in geologic systems, advection, rather than diffusion, appears to dominate the growth process.

Acknowledgements

The authors thank Don Winston and Annie Gellatly, University of Montana, for providing thin sections of the molar-tooth structure from Montana, and Larry Benson, U.S. Geological Survey, for providing the sediment core samples from Pyramid Lake, Nevada. The authors thank A. E. Blum (U.S. Geological Survey) and J. M. Neil (University of California, Davis) for their reviews of the original manuscript, and R.A. Ketcham (University of Texas) for helpful comments. The use of trade and product names in this paper is for identification purposes only, and does not constitute endorsement by the U.S. Geological Survey.

References Cited

Abegg, C.F., Stevens, J.D., and Larson, M.A. (1968) Crystal size distributions in continuous crystallizers when growth rate is size dependent. American Institute of Chemical Engineers Journal, 14, 118-122.

Benjamin, J.R., and Cornell, C.A. (1970) Probability, Statistics, and Design for Civil Engineers. 684 p., McGraw-Hill Book Co., New York.

Bennema, P. (1967) Analysis of crystal growth models for slightly supersaturated solutions. Journal of Crystal Growth, 1, 278-286.

Bennema, P. (1984) Spiral growth and surface roughening: Developments since Burton, Cabrera and Frank. Journal of Crystal Growth, 69, 182-197.

Bennett, P. (1962) Product size distribution in commercial crystallizers. Chemical Engineering Progress, 58, 76-80.

Berglund, K.A., Kaufman, E.L., and Larson, M.A. (1983) Growth of contact nuclei of potassium nitrate. American Institute of Chemical Engineers Journal, 29, 867-869.

Bove, D.J., Eberl, D.D., McCarty, D.K., and Meeker, G.P. (2002) Characterization and modeling of illite crystal particles and growth mechanisms in a zoned hydrothermal deposit, Lake City, Colorado. American Mineralogist, 87, 1546-1556.

Canning T.F., and Randolph A.D. (1967) Some aspects of crystallization theory: Systems that violate McCabe's delta L law. American Institute of Chemical Engineers Journal, 13, 5-10.

Eberl D.D., Drits V.A., and Srodon, J. (1998) Deducing growth mechanisms for minerals from the shapes of crystal size distributions. American Journal of Science, 298, 499-533.

Eberl, D.D., Drits, V.A., and Srodon, J. (2000) User's guide to Galoper—a program for simulating the shapes of crystal size distributions—and associated programs. 44 p., U.S. Geological Survey Open-File Report 00-505.

Eberl, D.D., Kile, D.E., and Drits, V.A. (2002a) On geological interpretations of crystal size distributions: Constant versus proportionate growth. American Mineralogist, 87, 1235-1241.

Eberl, D.D., Kile, D.E., and Hoch, A.R. (2002b) Crystallization of powders having uniform particle sizes by Ostwald ripening at large levels of supersaturation. U.S. Patent 6,379,459, April 30, 2002.

Exner H.E., and Lukas H.L. (1971) The experimental verification of the stationary Wagner-Lifshitz distribution of coarse particles. Metallography, 4, 325-338.

Furniss, G., Rittel, J.F., and Winston, D. (1998) Gas bubble and expansion crack origin of "molar-tooth" calcite structures in the Middle Proterozoic Belt subgroup, western Montana. Journal of Sedimentary Research, 68, 104-114.

Garside J., and Jancic, S.J. (1976). Growth and dissolution of potash alum crystals in the subsieve size range. American Institute of Chemical Engineers Journal, 22, 887-984.

Garside, J., Phillips, V.R., and Mukland, B.S. (1976) On size-dependent crystal growth. Industrial & Engineering Chemistry, Fundamentals, 15, 230-233.

Henisch, H.K. (1988) Crystals in Gels and Liesegang Rings, 197 p. Cambridge University Press, New York.

Holden, A., and Singer, P. (1960) Crystals and Crystal Growing, 320 p. Doubleday & Co., Inc., Garden City, New York.

Jones, A.G., Budz, J., and Mullin, J.W. (1986) Crystallization kinetics of potassium sulfate in an MSMPR agitated vessel. American Institute of Chemical Engineers Journal, 32, 2002-2009.

Jones, C.M., and Larson, M.A. (1999) Characterizing growth-rate dispersion of $NaNO_3$ secondary nuclei. American Institute of Chemical Engineers Journal, 45, 2128-2135.

Jones, C.M., and Larson, M.A. (2000) Using dislocations and integral strain to model the growth rates of secondary nuclei. Chemical Engineering Science, 55, 2563-2570.

Kile D.E., and Eberl D.D. (1999) Crystal growth in miarolitic cavities in the Lake George ring complex and vicinity, Colorado. American Mineralogist, 84, 718-724.

Kile, D.E., Eberl, D.D., Hoch, A.R., and Reddy, M.M. (2000) An assessment of calcite crystal growth mechanisms based on crystal size distributions. Geochimica et Cosmochimica Acta, 64, 2937-2950.

Kirkpatrick, R.J. (1981) Kinetics of crystallization of igneous rocks. In A.C. Lasaga and R.J. Kirkpatrick, Eds., Kinetics of geochemical processes, p. 321-398. Mineralogical Society of America, Reviews in Mineralogy.

Kretz, R. (1966) Grain-size distribution for certain metamorphic minerals in relation to nucleation and growth. Journal of Geology, 74, 147-173.

Krumbein W. C., and Graybill F. A. (1965) An Introduction to Statistical Models in Geology, 475 p. McGraw-Hill Book Co.

Makowitz A., and Sibley D.F. (1999) Crystal growth mechanisms of quartz overgrowths in a Cambrian quartz arenite. In Abstracts with Programs, 31, Annual Geological Society of America Meeting, October, 1999, Denver, Colorado, A-282.

Makowitz A., and Sibley D.F. (2001) Crystal growth mechanisms of quartz overgrowths in a Cambrian quartz arenite. Journal of Sedimentary Research, 71, 809-816.

Marsh B. D. (1988) Crystal size distribution (CSD) in rocks and the kinetics and dynamics of crystallization: I. Theory. Contributions to Mineralogy and Petrology, 99, 277-291.

McCabe W.L. (1929) Crystal growth in aqueous solutions. Industrial and Engineering Chemistry, 21, 30-33.

McCabe W.L., and Stevens R.P. (1951) Rate of growth of crystals in aqueous solutions. Chemical Engineering Progress, 47, 168-174.

McCoy, B.J. (2001) A new population balance model for crystal size distributions: Reversible, size-dependent growth and dissolution. Journal of Colloid and Interface Science, 240, 139-149.

Meth, C.E., and Carlson, W.D. (2002) Size-proportional garnet growth: An effect of precursor heterogeneity. Geological Society of America Abstracts with Programs, October 27-30, Denver, Colorado, 502.

Morse, J.W., and Wang, Q. (1996) Factors influencing the grain size distribution of authigenic minerals. American Journal of Science, 296, 989-1003.

Mullin, J.W. (1972) Crystallization, 2nd ed. 480 p., Butterworths, London.

Mullin, J.W., and Gaska, C. (1969) The growth and dissolution of potassium sulphate crystals in a fluidized bed crystallizer. The Canadian Journal of Chemical Engineering, 47, 483-489.

Nielsen A.E. (1964) Kinetics of Precipitation. 151 p., Pergamon Press.

Nordeng S.H., and Sibley D.F. (1996) A crystal growth rate equation for ancient dolomites: Evidence for millimeter-scale flux-limited growth. Journal of Sedimentary Research, 66, 477-481.

Ohara, M., and Reid, R.C. (1973) Modeling crystal growth rates from solution, 272 p. Prentice-Hall, New Jersey.

Ristic, R.I., Sherwood, J.N., and Shripathi, T. (1991) The role of dislocations and mechanical deformation in growth rate dispersion in potash alum crystals. In J. Garside, R.J. Davey, and A.G. Jones, Eds., Advances in Industrial Crystallization, 77-91.

Ristic , R.I., Sherwood, J.N., and Shripathi, T. (1997) Influence of tensile strain on growth of crystals of potash alum and sodium nitrate. Journal of Crystal Growth, 179, 194-204.

Srodon, J., Eberl, D.D., and Drits, V.A. (2000) Evolution of fundamental-particle size during illitization of smectite and implications for reaction mechanism. Clays and Clay Minerals, 48, 446-458.

Tai, C.Y., and Lin, C-H. (1987) Crystal growth kinetics of the two-step model. Journal of Crystal Growth, 82, 377-384.

Tai C.Y., and Yu, K.H. (1989) Growth kinetics of potassium alum crystal in a well-agitated vessel. Journal of Crystal Growth, 96, 849-855.

Tai C.Y., Chen, P-C., and Shih, S-M. (1993) Size-dependent growth and contact nucleation of calcite crystals. American Institute of Chemical Engineers Journal, 39, 1472-1482.

Tables

1. Growth parameters for alum experiments.
2. CSD parameters for calcite experiments and Precambrian molar tooth calcite.

Figures

1. Water-jacketed crystallization vessel with variable-speed stirrer for alum experiments.
2. Growth rate as a function of initial crystal size measured for (a) stirred and (b) unstirred systems for alum crystals.
3. CSD for calcite formed in a non-stirred system, with theoretical lognormal curve.
4. CSD measured for calcite grown in a 30-mm straight column: (a) upper Liesegang ring; (b) middle Liesegang ring; (c) lower Liesegang ring plotted using reduced axes.
5. Calcite crystals found in the Precambrian molar tooth structure: (a) measured CSD compared with the Galoper simulation (chi-square >20%) and the theoretical CSD expected for Ostwald ripening; (b) measured CSD with constant growth stage subtracted from the crystal sizes compared with the theoretical Ostwald curve (KS-test significance >10%).
6. Greigite (?) from Pyramid Lake, Nevada: (a) photomicrograph of crystals found within diatom tests, and (b) CSD measured for crystals compared with a Galoper simulation (χ^2 significance >20%).

Table 1. Growth parameters for alum experiments.
Nd = not determined

Experiment number	Stir rate (rpm)	T (°C)	Evap. rate (mL/h)	Average C (g/L)	σ *(Eq. 3)*	Slope[1] (Fig. 2)	Duration (h)
4-11-00	122[2]	24	Nd	Nd	Nd	0.284	1032
9-6-00	176	29.7	6.14	148.7	3.62	0.337	172
9-22-00	176	29.7	7.08	160.1	11.6	0.212	168
1-08-01	272	29.7	7.17	144.1	0.42	0.0648	144
2-28-01	171	29.3	1.83	Nd	Nd	0.0648	672
12-99	0	24	Nd	Nd	Nd	0.055	360
4-00	0	24	Nd	Nd	Nd	-0.030	1296
10-12-00	0	29.7	6.75	152.2	6.06	0.011	188
12-4-00	0	29.2	1.81	147.3	2.65	-0.019	432

[1]Slope determined from line drawn to exclude outliers.
[2]Magnetic stir bar used in place of propeller.

Table 2. CSD parameters for calcite experiments.
NA = not applicable

Experiment	Mean size, μm	Group size (nm)	α (from nm)	β^2	*Mean size at start of McCabe's growth (μm)*	β^2 at start of McCabe's growth	% McCabe's growth
Small fraction, 30-mm column	59.8	10000	10.97	0.057	NA	NA	NA
Medium fraction, 30-mm column	147.2	28000	11.87	0.064	NA	NA	NA
Large fraction, 30-mm column	312.9	26000	12.64	0.017	173.9	0.066	44
U-tube (gel) large fraction	565.5	50000	13.23	0.038	438.3	0.070	22
Calcite, "molar tooth"	13.3	1600	9.49	0.021	7.5	0.064	44
Calcite, unstirred	28.2	6300	10.14	0.227	NA	NA	NA

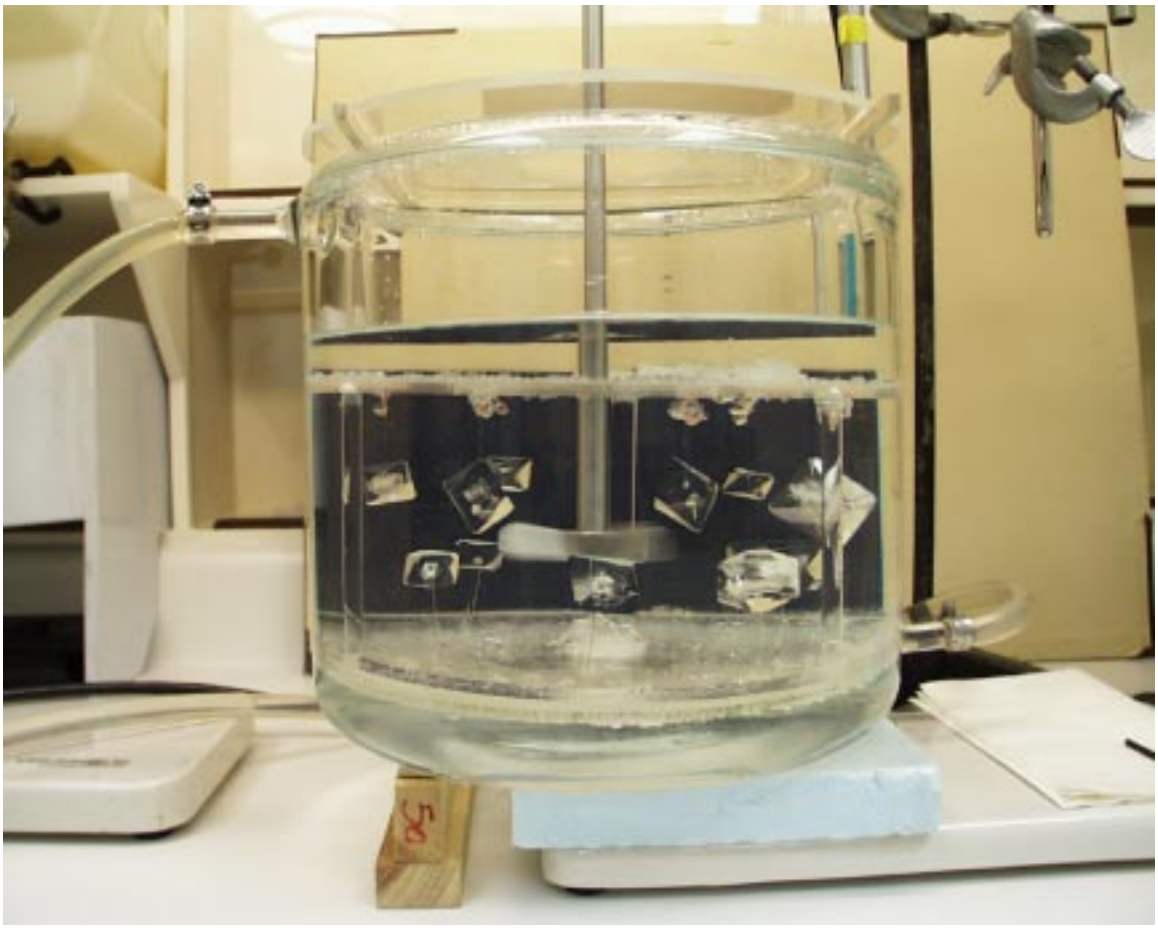

Figure 1

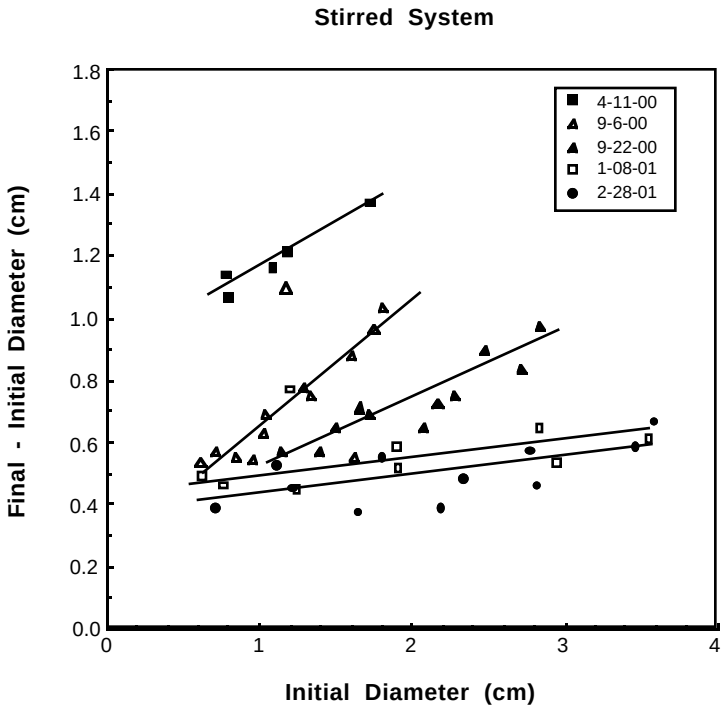
Stirred System
Final - Initial Diameter (cm)
Initial Diameter (cm)
4-11-00
9-6-00
9-22-00
1-08-01
2-28-01
0.0
0.2
0.4
0.6
0.8
1.0
1.2
1.4
1.6
1.8
0
1
2
3
4

Fig. 2a

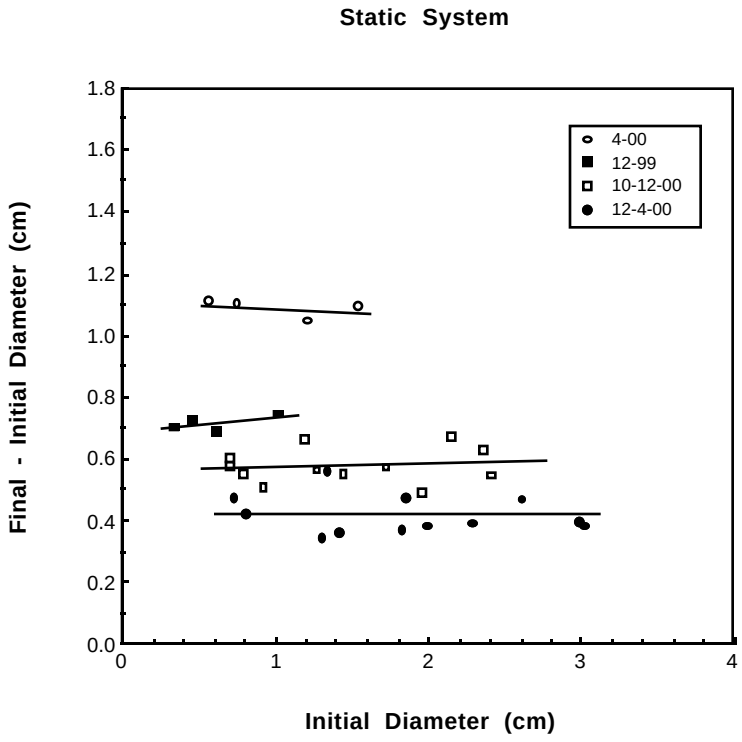
Static System
Final - Initial Diameter (cm)
Initial Diameter (cm)
4-00
12-99
10-12-00
12-4-00
0.0
0.2
0.4
0.6
0.8
1.0
1.2
1.4
1.6
1.8
0
1
2
3
4

Fig. 2b

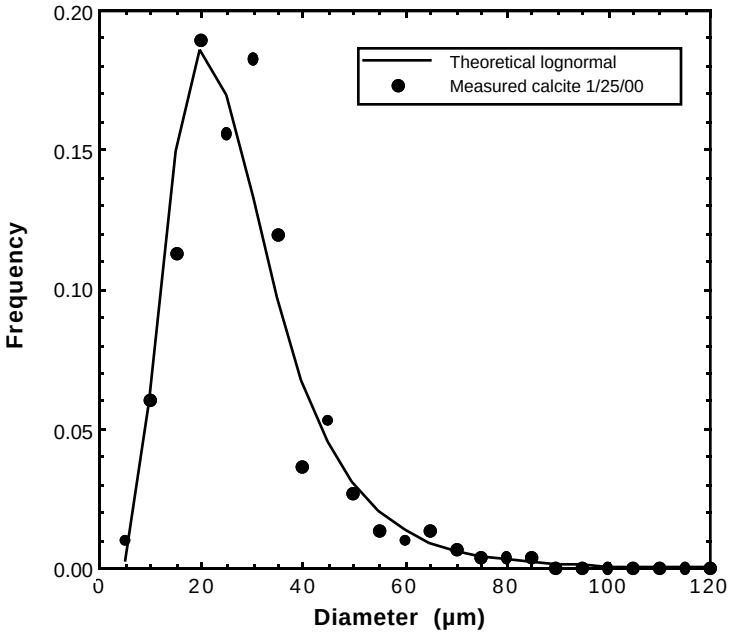
Theoretical lognormal
Measured calcite 1/25/00
Frequency
Diameter (µm)
0.00
0.05
0.10
0.15
0.20
0
20
40
60
80
100
120

Fig. 3

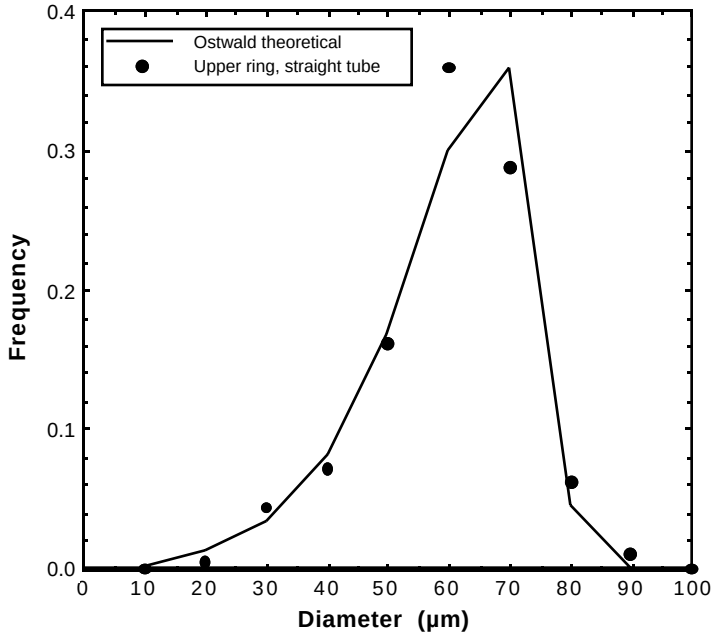
Ostwald theoretical
Upper ring, straight tube
Frequency
Diameter (µm)
0.0
0.1
0.2
0.3
0.4
0
10
20
30
40
50
60
70
80
90
100

Fig. 4a

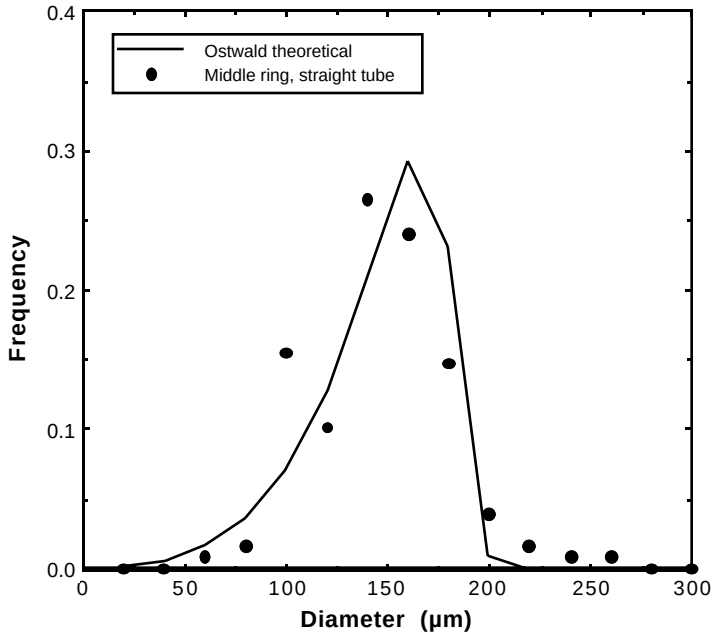
Ostwald theoretical
Middle ring, straight tube
Frequency
Diameter (μm)
0.0
0.1
0.2
0.3
0.4
0
50
100
150
200
250
300

Fig. 4b

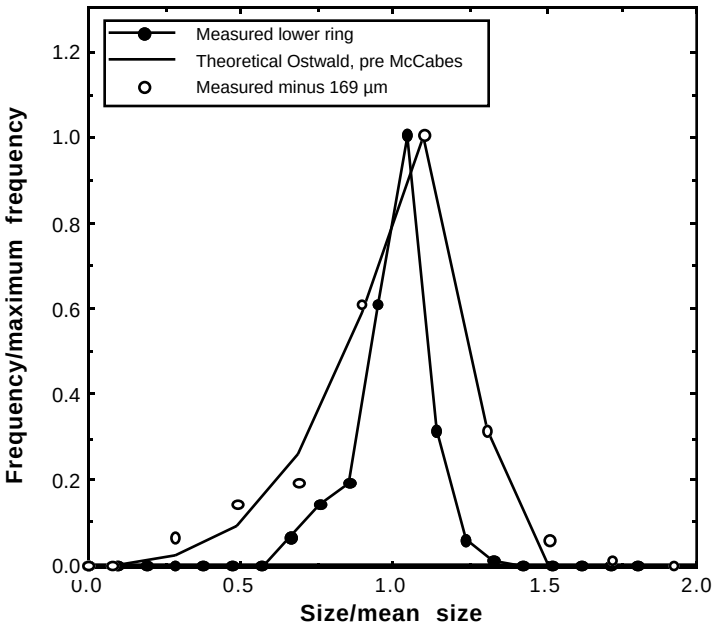
Measured lower ring
Theoretical Ostwald, pre McCabes
Measured minus 169 μm
Frequency/maximum frequency
Size/mean size
0.0
0.2
0.4
0.6
0.8
1.0
1.2
0.0
0.5
1.0
1.5
2.0

Fig. 4c

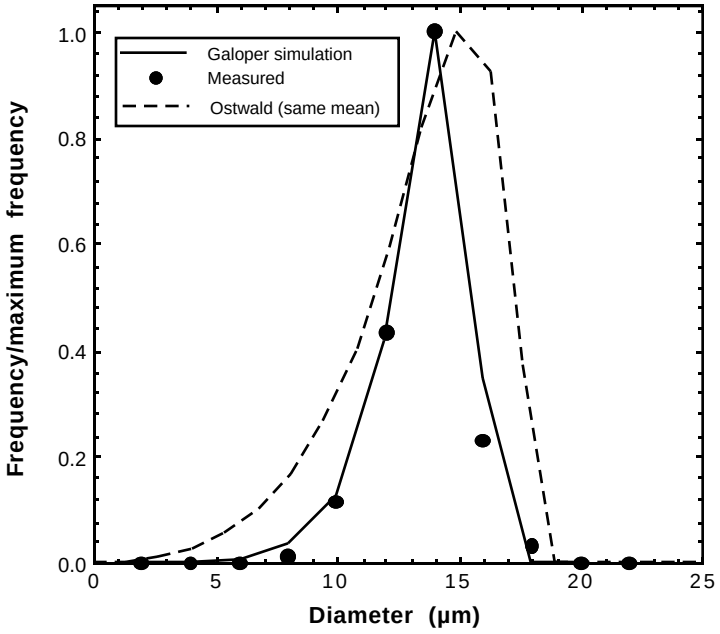
Galoper simulation
Measured
Ostwald (same mean)
Frequency/maximum frequency
Diameter (µm)
0.0
0.2
0.4
0.6
0.8
1.0
0
5
10
15
20
25

Fig. 5a

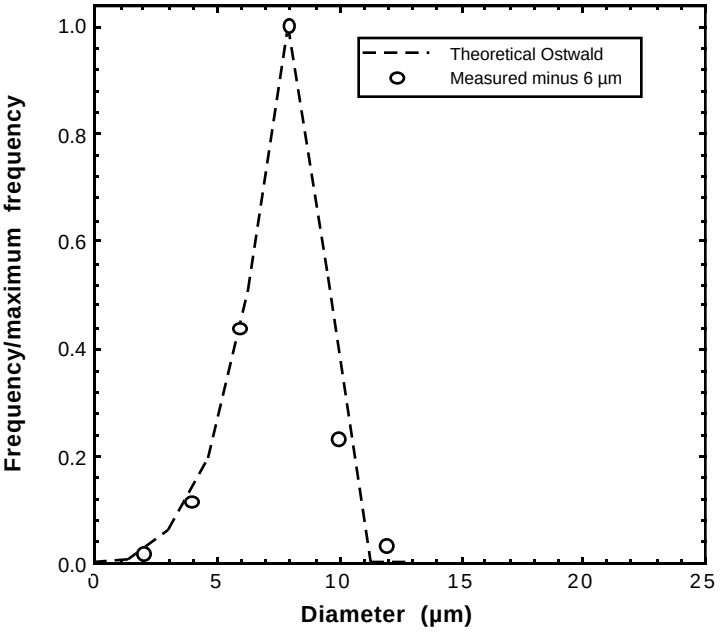
Theoretical Ostwald
Measured minus 6 µm
Frequency/maximum frequency
Diameter (µm)
0.0
0.2
0.4
0.6
0.8
1.0
0
5
10
15
20
25

Fig. 5b

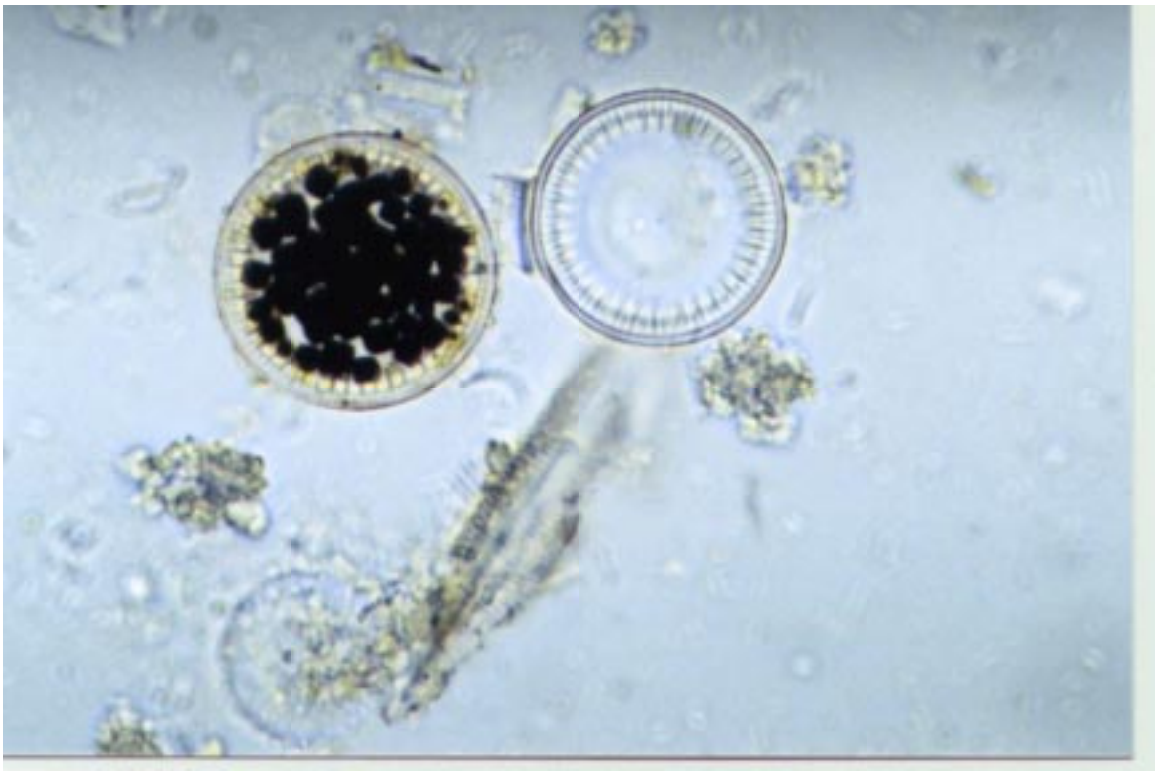

Figure 6a

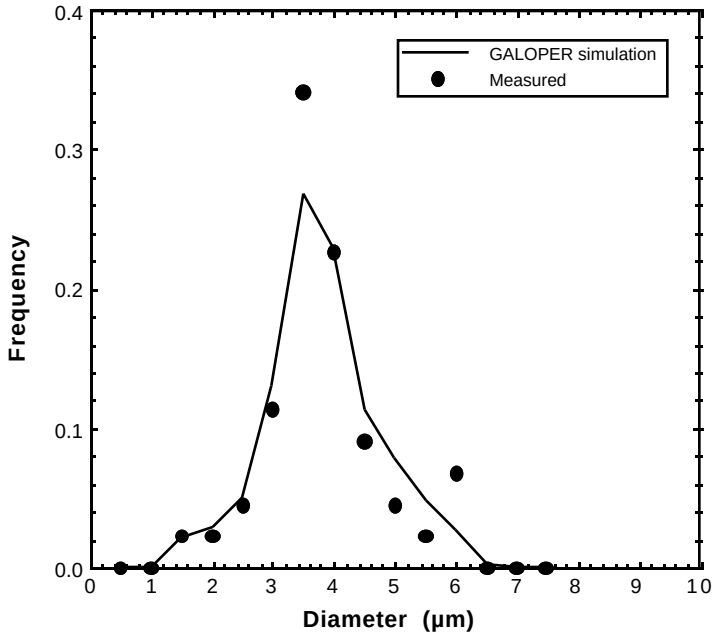

Fig. 6b